Geochemistry Geophysics Geosystems G3

Article
Volume 11, Number 10
21 October 2010
Q10012, doi:10.1029/2010GC003247
ISSN: 1525-2027

Published by AGU and the Geochemical Society

Upper mantle anisotropy and transition zone thickness beneath southeastern North America and implications for mantle dynamics

Maureen D. Long
Department of Geology and Geophysics, Yale University, PO Box 208109, New Haven, Connecticut 06520, USA (maureen.long@yale.edu)

Margaret H. Benoit
Department of Physics, College of New Jersey, PO Box 7718, Ewing, New Jersey 08628, USA

Martin C. Chapman and Scott D. King
Department of Geosciences, Virginia Polytechnic Institute and State University, 4044 Derring Hall, Blacksburg, Virginia 24061, USA

[1] A variety of models for mantle flow beneath southeastern North America have been proposed, including those that invoke westward driven return flow from the sinking Farallon slab, small-scale convective downwelling at the edge of the continental root, or the upward advective transport of volatiles from the deep slab through the upper mantle. We use shear wave splitting observations and receiver function analysis at broadband seismic stations in the southeastern United States to test several of these proposed mantle flow geometries. Near the coast, stations exhibit well-resolved null (no splitting) behavior for SKS phases over a range of back azimuths, consistent with either isotropic upper mantle or with a vertical axis of anisotropic symmetry. Farther inland we identify splitting with mainly NE–SW fast directions, consistent with asthenospheric shear due to absolute plate motion (APM), lithospheric anisotropy aligned with Appalachian tectonic structure, or a combination of these. Phase-weighted stacking of individual receiver functions allows us to place constraints on the timing of arrivals from the 410 and 660 km discontinuities and on average transition zone thickness beneath individual stations. At most stations we find transition zone thicknesses that are consistent with the global average (~240 km), with two stations showing evidence for a slightly thickened transition zone (~250 km). Our results are relevant for testing different models for mantle dynamics beneath the southeastern United States, but due to the sparse station coverage, we are unable to uniquely constrain the pattern of mantle flow beneath the region. Our SKS splitting observations support a model in which mantle flow is primarily vertical (either upwelling or downwelling) beneath the southeastern edge of the North American continent, in contrast to the likely horizontal, APM-driven flow beneath the continental interior. However, our receiver function analysis does not provide unequivocal support either for widespread hydration of the transition zone or for widespread thickening due to the downwelling of relatively cold mantle material. We expect that the necessary data to constrain such models more tightly can be obtained from the operation of denser seismic networks, including the Transportable Array and Flexible Array components of USArray.

Components: 13,000 words, 13 figures, 1 table.

Keywords: mantle flow; seismic anisotropy; shear wave splitting; receiver functions; converted waves; North American continent.

Index Terms: 7208 Seismology: Mantle (1212, 1213, 8124); 7203 Seismology: Body waves; 8120 Tectonophysics: Dynamics of lithosphere and mantle: general (1213).

Received 4 June 2010; **Revised** 23 August 2010; **Accepted** 26 August 2010; **Published** 21 October 2010.

Long, M. D., M. H. Benoit, M. C. Chapman, and S. D. King (2010), Upper mantle anisotropy and transition zone thickness beneath southeastern North America and implications for mantle dynamics, *Geochem. Geophys. Geosyst.*, *11*, Q10012, doi:10.1029/2010GC003247.

1. Introduction

[2] The character of the mantle flow field beneath stable continental interiors has been extensively studied [e.g., *Fouch and Rondenay*, 2006, and references therein], but only a few studies have addressed the geometry of mantle flow beneath passive continental margins [e.g., *Farrington et al.*, 2010]. Three recent studies have proposed models for mantle dynamics and upper mantle flow geometries beneath the continental margin of southeastern North America. One model invokes the flow field associated with the sinking of the Farallon slab to provide the lithospheric stresses required to produce the 1811–1812 earthquake sequence at the New Madrid Seismic Zone [*Forte et al.*, 2007]. A second model seeks to explain an observed slow shear wave velocity anomaly in the upper mantle roughly parallel to the Appalachian mountains by dehydration of the Farallon slab and upward transport of the resulting volatiles [*van der Lee et al.*, 2008]. Finally, small-scale convection driven by the deep lithospheric root associated with the North American craton has been suggested as the cause of the Bermuda hot spot [*King*, 2007]. Observations from broadband seismic stations in southeastern North America may be used to discriminate among these different mantle flow geometries. Here we use shear wave splitting observations and receiver function analysis of mantle discontinuity structure to test the predictions made by each of these models.

[3] The effect of the subducting Farallon slab on large-scale mantle flow beneath the North American continent has been considered by a number of numerical modeling studies [e.g., *Conrad et al.*, 2004; *Forte et al.*, 2007; *Moucha et al.*, 2008; *Liu et al.*, 2008; *Spasojevic et al.*, 2010]; the model of *Forte et al.* [2007] specifically addresses the geometry of mantle flow beneath central and eastern North America. Using instantaneous viscous flow models driven by density anomalies calculated from seismic tomographic anomalies, *Forte et al.* [2007] showed that downwelling mantle flow driven by the Farallon slab produces localized viscous flow and high lithospheric stresses beneath the New Madrid Seismic Zone. They argued that the mantle flow driven by the sinking Farallon slab will produce a surface depression and that this may induce seismicity in a process similar to previously proposed crustal loading mechanisms [e.g., *Grana and Richardson*, 1996]. Their models predict westward horizontal flow in the upper mantle beneath eastern North America and this flow should in turn lead to the development of a horizontally aligned olivine aligned texture that should be reflected in shear wave splitting observations (Figure 1a). Similar predictions of present-day westward horizontal mantle flow beneath the southeastern United States are made by time-dependent models that take into account the evolution of the Farallon slab over the past 100 Myr [*Liu et al.*, 2008].

[4] *van der Lee et al.* [2008] interpreted an observed slow shear wave velocity anomaly in regional seismic waveform tomography beneath the eastern North America parallel to the margin as a hydrous upwelling associated with dehydration of the Farallon slab as it descends through the transition zone into the lower mantle [e.g., *Bercovici and Karato*, 2003]. They envision this hydrated mantle to be buoyant and thus their model predicts vertical upwelling flow beneath the eastern North American margin and associated surface uplift (Figure 1b). Localized upwelling beneath southeastern North America has also been predicted from global instantaneous flow models [*Spasojevic et al.*, 2010]. Such vertical mantle flow would result in upper mantle anisotropy with a vertical axis of symmetry, as long as there was a lateral gradient in vertical velocities that would result in a vertically oriented axis of maximum finite strain. A vertical axis of hexagonal anisotropic symmetry would in turn manifest itself in a lack of shear wave splitting for vertically propagating phases such as SKS. Under hydrous conditions, the transformation of olivine to wadsleyite (i.e., the 410 km discontinuity) occurs at lower pressures than under anhydrous conditions [*Wood*, 1995; *Smyth and Frost*, 2002]; this model, therefore, predicts an elevated 410 km discontinuity. The 660 km discontinuity, in contrast, is expected to deepen slightly under hydrous conditions [*Higo et al.*, 2001], although the effect of water on the phase transition pressure is considerably smaller

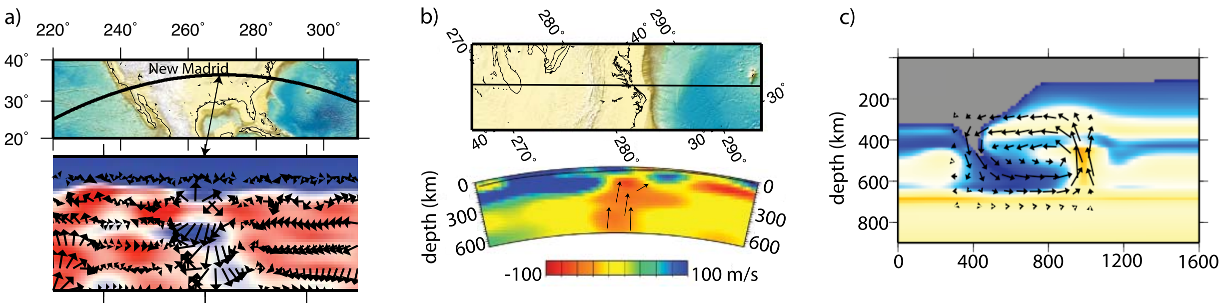

Figure 1. Three proposed flow geometries beneath the southeastern North America continental margin are illustrated. (a) A cross section of density-driven mantle flow velocities beneath North America (map view) predicted from a tomographic model (color contours). *Forte et al.* [2007] suggest that the sinking Farallon slab provides compressive stresses above New Madrid and westward horizontal mantle flow beneath the southeastern United States. (b) A slow shear wave velocity anomaly in the tomographic surface wave model NA04 [*van der Lee and Frederiksen*, 2005] beneath southeastern NA (map view). *van der Lee et al.* [2008] suggest that this anomaly corresponds to a volatile-rich region associated with vertical transport of volatiles from the Farallon slab at depth; the vertical flow predicted by this model is indicated by the arrows. (c) The predicted flow field from small-scale edge-driven convection, as in the work by *King and Anderson* [1998]. The EDC model would predict downwelling at the edge of the North American cratonic interior. *King* [2007] hypothesized that the corresponding upwelling limb of the convection cell may correspond to the Bermuda swell.

than for the 410. A transition zone with uniform hydration throughout would therefore be expected to be thicker than an anhydrous one.

[5] *King and Anderson* [1998] proposed that sharp boundaries in lithospheric structure, for example at the edges of cratons, could nucleate small-scale convection. *King and Ritsema* [2000] found evidence for small-scale convection beneath the West African craton and speculated that this is the source of African hot spots. *King* [2007] showed that the Bermuda hot spot is geometrically favorable for a similar small-scale convective origin and the margin of eastern North America would be a likely nucleation point for small-scale convection (Figure 1c), with a localized cold downwelling driving a corresponding upwelling on the other limb of the convection cell. Detection of a thick transition zone (associated with an elevated 410 km discontinuity and depressed 660 km discontinuity) consistent with cold, downwelling mantle and the absence of birefringence on SKS records (consistent with vertical flow) beneath southeastern North America would be consistent with edge-driven convection.

[6] A clear indication of mantle structure and flow could help discriminate between these three proposed mantle flow geometries; however, there is significantly less seismic activity in southeastern North America than western North America and, perhaps not surprisingly, few existing broadband seismic stations (Figure 2 and Table 1). As a result, our understanding of mantle structure and dynamics beneath southeastern North America is limited. Here we present SKS splitting measurements (fast directions and delay times) and estimates of transition zone thickness from P wave receiver function stacks of mantle discontinuity structure from available permanent broadband seismic data from southeastern North America and compare these observations with the predictions for the proposed upper mantle flow geometries described above. The goal is to determine whether the current broadband data are sufficient to discriminate among these proposed models for mantle dynamics and, if so, to place constraints on the character of mantle flow beneath the southeastern United States.

2. SKS Splitting: Methods and Results

[7] We examined the shear wave splitting of SKS phases recorded at 11 stations located in southeastern North America (Figure 2 and Table 1). Nine of these stations are currently operating; CEH and GWDE ceased operation in 2001. We examined at least 5 years' worth of data for each station, except for TZTN and CNNC (which began operation in February 2005 and June 2006, respectively). SKS phases were selected for analysis from events of magnitude ≥5.8 at epicentral distances between 88° and 120° (see event map in Figure 3). Horizontal seismograms were examined after a bandpass filter (corner frequencies = 0.1 and 0.02 Hz) was applied and clear SKS arrivals with high signal-to-noise ratios and good waveform clarity were

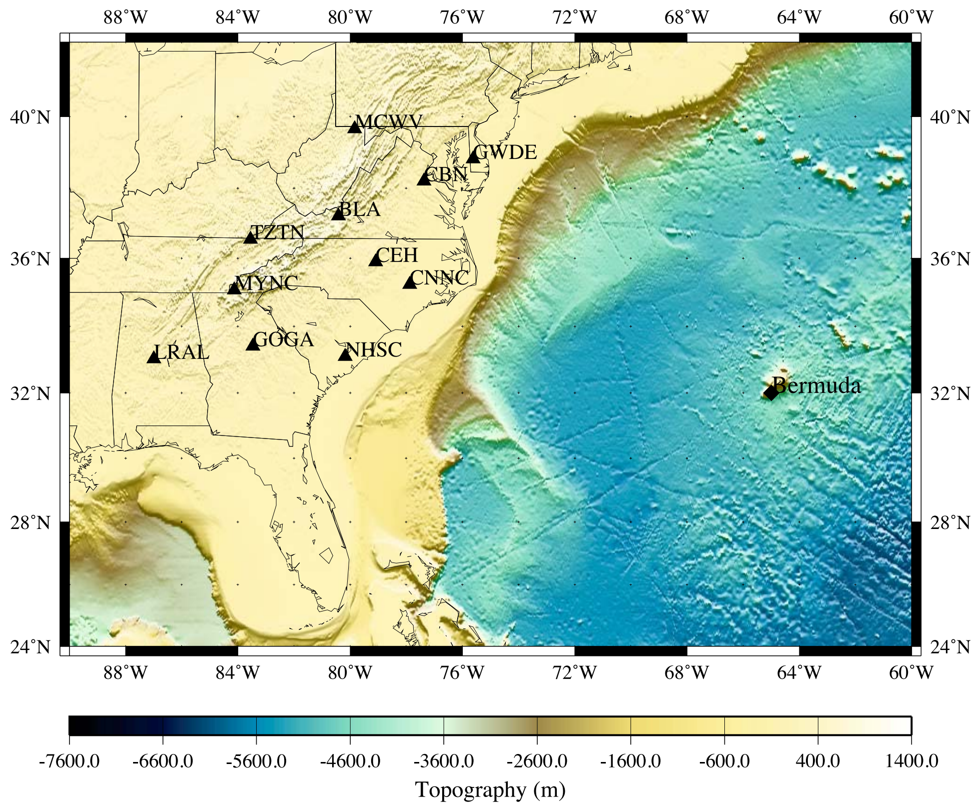

Figure 2. Permanent or long-running broadband stations located in southeastern NA used in this study. Topography, bathymetry, and the location of the Bermuda swell are shown.

selected for splitting analysis. (In approximately 10% of cases, we adjusted the corner frequencies slightly to optimize waveform clarity, as in the work by *Long et al.* [2009].) We manually windowed around the SKS phase to select a time window for splitting analysis, with the windows covering at least one full period of the SKS arrival.

[8] In order to ensure the highest-quality data set possible, we used two simultaneous measurement methods (the rotation-correlation method and the transverse component minimization method; for details, see *Long and Silver* [2009], and references therein) and only retained nonnull measurements for which the two methods agreed (within the 2σ error ellipses). Previous studies have shown that the two methods can disagree in the presence of noise [e.g., *Long and van der Hilst*, 2005] or when the incoming polarization is close to a null direction [e.g., *Wüstefeld and Bokelmann*, 2007]. The

Table 1. Names, Locations, and Times of Operation of Broadband Stations Used in This Study, Along With the Number of Individual Receiver Functions That Were Used to Compute the Stacks Shown in Figure 10[a]

Station	Location	Latitude	Longitude	Start Date	End Date	RF
BLA	Blacksburg, VA	37.21	−80.42	24 Jun 1994	–	146
CBN	Corbin, VA	38.20	−77.37	15 Jun 2001	–	–
CEH	Chapel Hill, NC	35.89	−79.09	29 Mar 1991	26 Feb 2001	53
CNNC	Cliffs of the Neuse, NC	35.24	−77.89	26 Jun 2006	–	–
GOGA	Godfrey, GA	33.41	−83.47	9 Mar 1993	–	47
GWDE	Greenwood, DE	38.83	−75.62	7 Sep 1995	11 May 2001	–
LRAL	Lakeview Retreat, AL	33.03	−87.00	2 Jul 2001	–	44
MCWV	Mont Chateau, WV	39.66	−79.85	28 Mar 1991	–	55
MYNC	Murphy, NC	35.07	−84.13	31 Mar 1993	–	25
NHSC	New Hope, SC	33.11	−80.18	1 May 2001	–	28
TZTN	Tazewell, TN	36.54	−83.55	23 Feb 2005	–	55

[a]Note that station MYNC is still operating but has suffered from technical problems since early 2003, and the data archive is incomplete after this date.

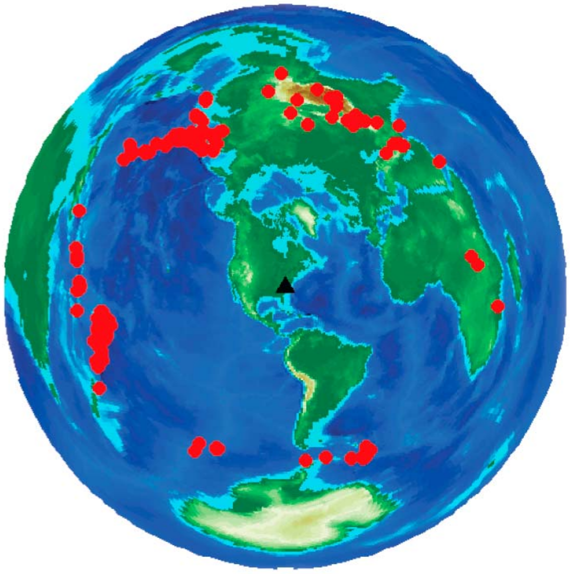

Figure 3. Map of events that yielded at least one usable (null or nonnull) SKS splitting measurement at the 11 stations examined in this study.

splitting measurements were ranked as "good" or "fair" according to the following criteria (following *Long et al.* [2009]): measurements with clearly elliptical uncorrected particle motion and linear or very nearly linear corrected particle motion, good agreement between measurement methods, and small errors (less than ±15° in fast direction and ±0.3 s in delay time for the transverse component minimization method) were ranked as "good," while measurements with larger errors (up to ±30° and ±1.0 s) and lower signal-to-noise ratios were ranked as "fair." While the SKS signal-to-noise ratio and formal measurement errors were quantified for each measurement, our overall quality measurement is necessarily more qualitative, and follows the example of previous studies [e.g., *Pozgay et al.*, 2007; *Long et al.*, 2009]. We classified as null those measurements with high signal-to-noise ratio, good waveform clarity, and linear or nearly linear initial particle motion. We did not classify noisy, complex waveforms as null measurements; only clear SKS arrivals with linear uncorrected particle motion in the direction of the back azimuth were classified as nulls. Examples of null and nonnull "good" quality splitting measurements using both measurement methods for station LRAL are shown in Figure 4. This procedure yielded a total of 24 nonnull measurements and 311 null measurements at 10 stations (station GWDE did not yield any usable results) from 171 events. Of the 24 nonnull measurements, 7 were classified as "good," and the rest "fair." Maps showing both null and nonnull measurements are shown in Figure 5.

[9] The most striking first-order observation is the preponderance of null splitting measurements at stations in the southeastern United States. Of the ten stations that yielded usable measurements, four of them exhibited only null measurements, and at two of these (NHSC and GOGA) well-constrained nulls were measured over a fairly wide range of back azimuths. Stations CNNC and CBN each yielded a large number of nulls, and particularly at station CBN, these nulls cover a wide range of back azimuths; however, CNNC and CBN each yielded one well-constrained nonnull measurement as well. Only four stations (LRAL, TZTN, BLA, and MCWV) yielded more than one nonnull measurement. These stations are all located relatively far from the coast; we observe a striking difference between splitting patterns at these "interior" stations and those observed at stations located closer to the edge of the continental margin, which tend to be nearly or completely dominated by null splitting (CBN, CNNC, NHSC, and GOGA). The fast directions at LRAL, TZTN, BLA, and MCWV cluster around an average value that is approximately NE-SW, although there is significant scatter in individual measurements, particularly at MCWV. Large numbers of null measurements were also identified at these stations; at TZTN and BLA, the nulls cover a wide back azimuthal range. Our results are broadly consistent with an earlier study by *Barruol et al.* [1997], who identified station CEH as a null station and found roughly NE-SW average fast directions at MCWV and BLA. *Barruol et al.* [1997] identified NE-SW fast directions at station MYNC; our study yielded only null measurements at this station, but the back azimuthal distribution of these nulls is consistent with anisotropy with a NE–SW fast symmetry axis.

[10] We observe a conspicuous difference in splitting behavior between stations located in the continental interior (MCWV, BLA, TZTN, and LRAL), which tend to exhibit splitting with a roughly NE-SW fast direction, and stations located closer to the coast (CBN, CNNC, NHSC, and GOGA), which tend to be dominated by null measurements. A key question, therefore, is whether this difference in observed splitting behavior is due to difference in anisotropic structure beneath the stations or merely due to differences in data quality. With the exceptions of stations CEH and GWDE, at which data quality was generally poor, we did not observe any qualitative difference in data quality between inland stations and those located closer to the coast, and at

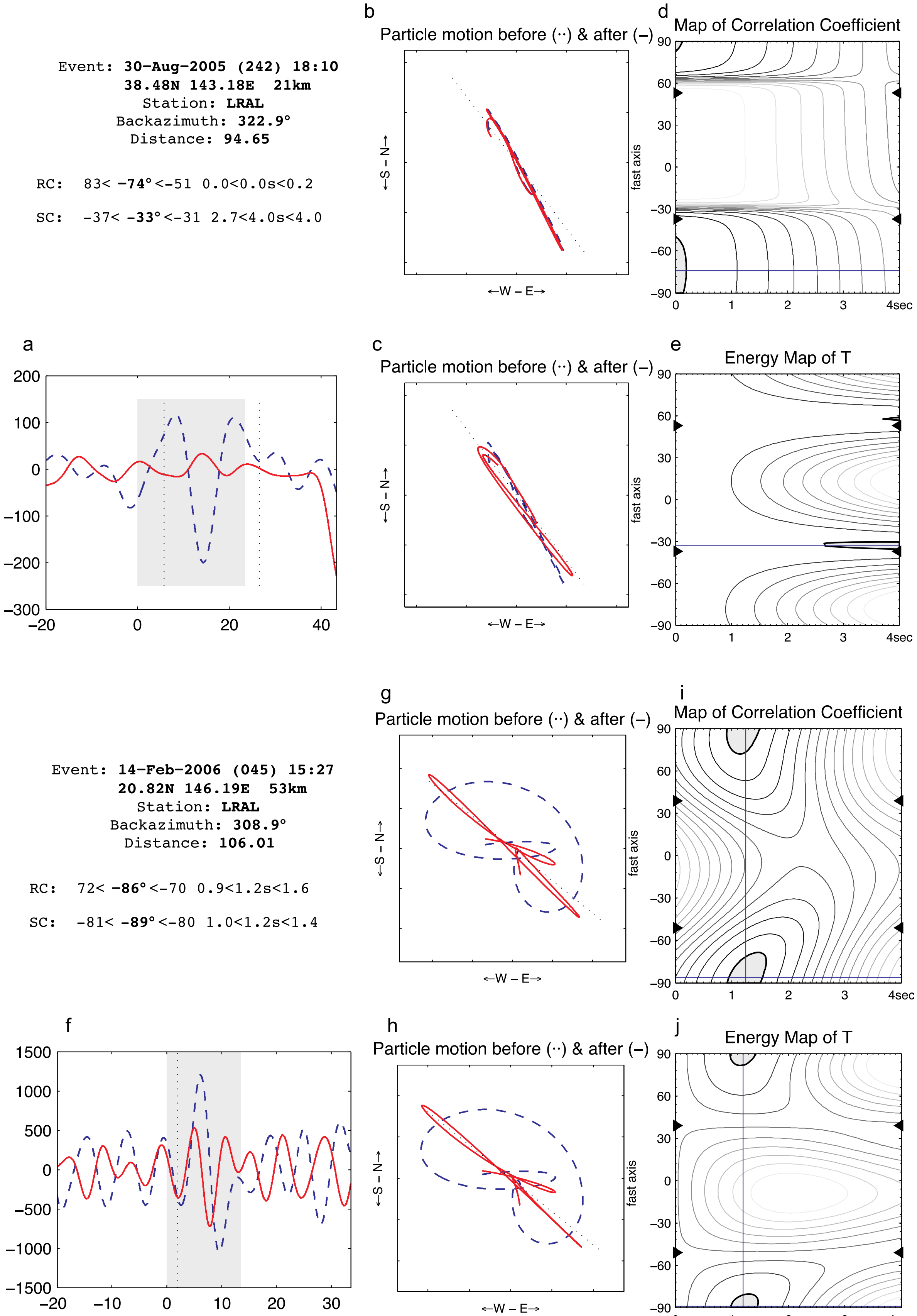

Event: 30-Aug-2005 (242) 18:10
38.48N 143.18E 21km
Station: LRAL
Backazimuth: 322.9°
Distance: 94.65
RC: 83< -74°<-51 0.0<0.0s<0.2
SC: -37< -33°<-31 2.7<4.0s<4.0
a
b
Particle motion before (··) & after (–)
c
d
Map of Correlation Coefficient
e
Energy Map of T
fast axis
←S – N→
←W – E→
4sec
Event: 14-Feb-2006 (045) 15:27
20.82N 146.19E 53km
Station: LRAL
Backazimuth: 308.9°
Distance: 106.01
RC: 72< -86°<-70 0.9<1.2s<1.6
SC: -81< -89°<-80 1.0<1.2s<1.4
f
g
h
i
j

Figure 4

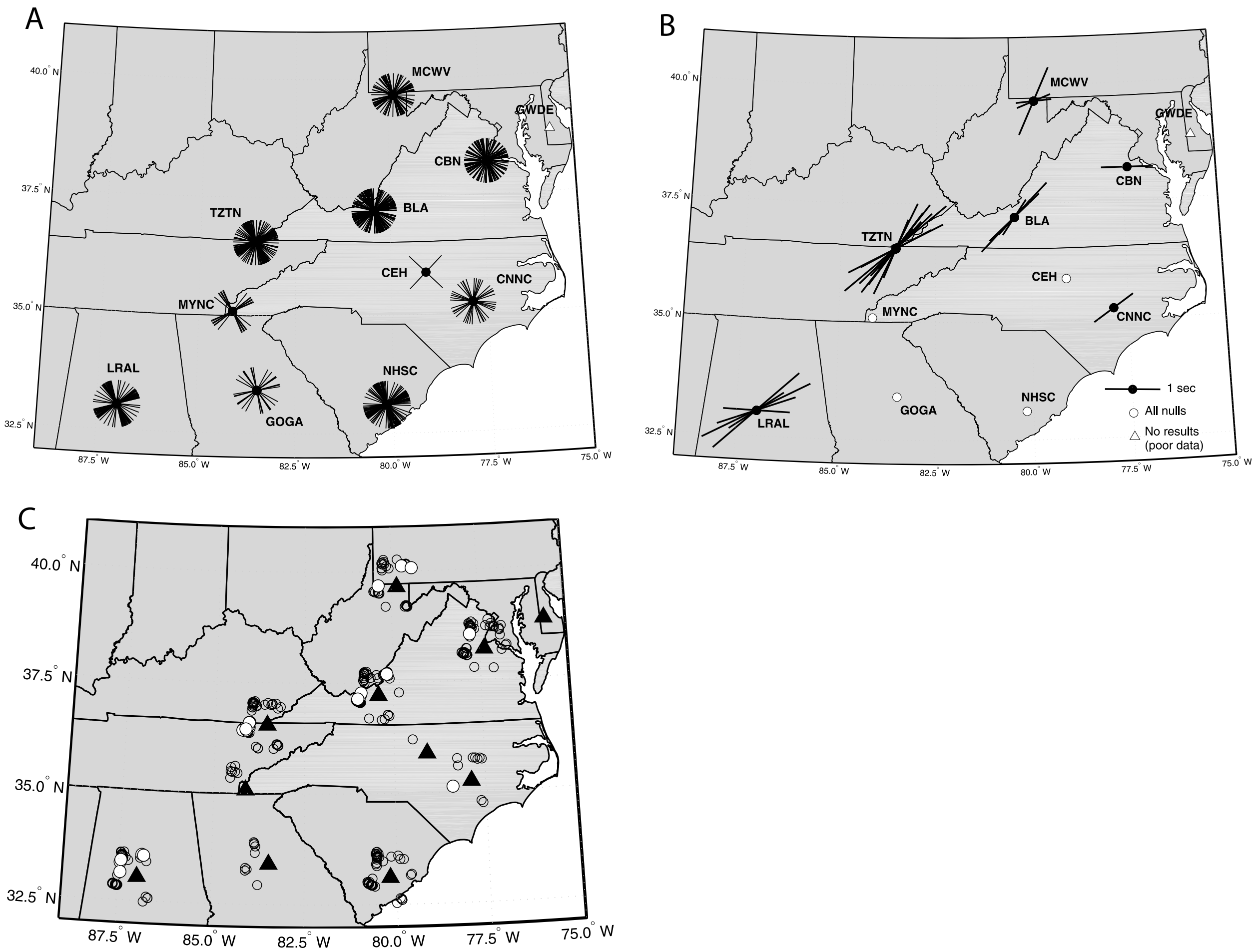

Figure 5. SKS splitting analysis results. (a) Map of null splitting measurements. Nulls are plotted at the station location as crosses, with one arm of the cross parallel to the incoming polarization azimuth (equivalent to the back azimuth for SKS phases) and the other arm orthogonal to it. Station GWDE, which had insufficient data quality, is shown with a triangle. (b) Map of individual nonnull splitting measurements plotted at the station location. Splitting parameters are represented as bars oriented parallel to the fast polarization direction, with the length of the bar scaled to the delay time. Stations which yielded only null results are shown with a circle; station GWDE is shown with a triangle. (c) Map of the 410 km pierce points for all null (black circles) and nonnull (white circles) measurements. Station locations are shown with triangles.

Figure 4. Examples of typical null and nonnull splitting measurements, both at station LRAL, obtained using SplitLab [*Wüstefeld et al.*, 2008]. (a–e) A well-resolved, "good" quality null measurement from an event located in the Japan subduction zone. Figure 4a shows the uncorrected radial (blue dashed line) and transverse (red solid line) components, with the gray region indicating the time window used in the measurement. Figures 4b and 4c indicate the uncorrected (blue dashed) and corrected (red solid) particle motions obtained using the rotation-correlation method (Figure 4b) and the transverse component minimization method (Figure 4c), respectively. The dotted line indicates the back azimuth; the initial particle motion is linear and nearly aligned with the back azimuth, which indicates null splitting. The error contours for each method are shown in Figures 4d and 4e. (f–j) A well-resolved, "good" quality nonnull measurement from an event located in the Marianas subduction zone. The panels are as in Figures 4a–4e. This arrival exhibits significant energy above the noise level on the transverse component (Figure 4f), and the uncorrected particle motion is elliptical while the corrected particle motion is nearly linear (Figures 4g and 4h). The two methods yield very similar estimates for the best fitting splitting parameters, namely, $\varphi = 72° < -86° < -70°$ and $\delta t = 0.9$ s < 1.2 s < 1.6 s using the rotation-correlation method and $\varphi = 81° < -89° < -80°$ and $\delta t = 1.0$ s < 1.2 s < 1.4 s using the transverse component minimization method (error bars are 2σ).

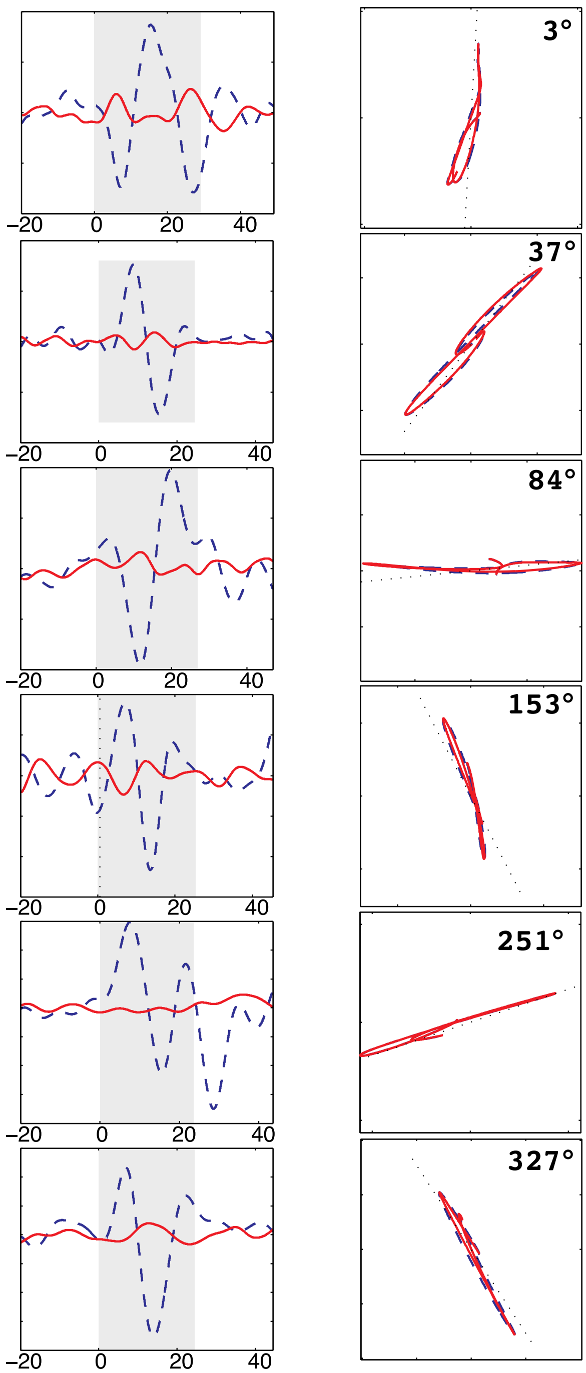

Figure 6. Splitting behavior over a range of back azimuths at station NHSC, which exhibits only null splitting. Typical waveforms and particle motion diagrams at six different back azimuths are shown. (left) The uncorrected radial and transverse components (*x* axis labels indicate time in s) and (right) the particle motion diagrams. The back azimuth is shown in the top right corner of each of the panels in Figure 6 (right).

several of the stations located near the continental margin, a large number of well-constrained high-quality nulls were observed (e.g., 49 nulls at NHSC and 57 at CBN). In order to demonstrate this data quality, a selection of waveforms associated with high-quality null splitting measurements at station NHSC at a variety of back azimuths are shown in Figure 6; Figure 6 clearly demonstrates that high-quality null measurements are observed over a large range of back azimuths at this station.

[11] A striking difference in splitting behavior between Appalachian and coastal stations can be seen in Figure 5, but to provide further confirmation of this observation, we interrogated our SKS splitting data set to look for events that were clearly recorded at both coastal and inland stations. We identified 4 high-quality events that were recorded at 6 or more of the stations, but all of these were from northwesterly back azimuths and exhibited uniformly null splitting at all stations. However, we identified several events for which we obtained well-constrained splitting parameters at 3 or more stations that exhibited different splitting behavior for Appalachian and coastal stations. For example, an event from the northern Tonga subduction zone on 02/02/06 exhibited null splitting at stations CBN and NHSC, but exhibited splitting with $\varphi = 47°$, $\delta t = 1.5$ s at station TZTN. We also identified many examples of events that were recorded at one inland station and one coastal station and show discrepancies. Three of these examples are shown in Figure 7, which shows uncorrected and corrected particle motion diagrams for events that exhibit significant splitting at an Appalachian station (LRAL or TZTN in the examples shown) and null splitting at a coastal station (CBN or NSHC).

[12] While the observation of significant (generally ~0.5–1.5 s) SKS splitting with a generally NE-SW fast direction at inland stations is robust, we emphasize that the splitting patterns at these stations are fairly complex, and the anisotropic structure beneath these stations is likely to be more complex than a simple, single horizontal layer of anisotropy. In Figure 8, we show the back azimuthal variation in observed splitting behavior (including null and nonnull measurements) for stations MCWV, BLA, TZTN, and LRAL. A large number of well-constrained null measurements are observed at these stations, and nonnull splitting is only observed at a limited number of back azimuths at most stations (most notably TZTN, which has a large number of well-constrained nonnull measurements that occur over a very small range of back azimuths). In a few cases (two at station BLA and one at MCWV;

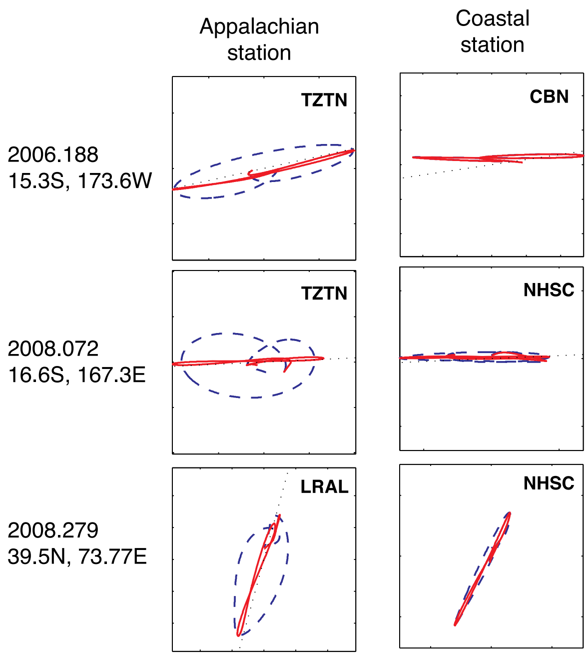

Figure 7. Examples of SKS arrivals from three different events that show different splitting behavior at Appalachian and coastal stations. (left) Uncorrected (blue dashed) and corrected (red solid) particle motion for the SKS phase for Appalachian stations. (right) Corresponding particle motion for coastal stations. The event date and location is shown to the left of each set of diagrams; the station name is shown in the top right corner.

see Figure 8), nonnull measurements coexist with null measurements at nearly identical back azimuths. These discrepancies can likely be explained by either particularly noisy data that led to a poor estimate of splitting parameters and underestimated measurement errors, or to small deviations of the actual initial polarization of the SKS phase from the back azimuth due to lateral (isotropic) heterogeneity somewhere along the raypath. The complexity evident in the patterns shown in Figure 8 argues for complex anisotropy beneath this region. This complex structure may take the form of small-scale lateral heterogeneity in the crust or shallow mantle, or it may be indicative of multiple layers of anisotropy (in the crust, mantle lithosphere, and/or asthenosphere) with different geometries. For complex anisotropic structure at depth, small differences in initial polarization can lead to very different splitting behavior, as observed at all four stations shown in Figure 8.

[13] The limited spatial coverage of permanent or long-running broadband stations and the complexity in splitting patterns observed at many stations in this study make a unique interpretation for upper mantle anisotropy beneath the region difficult. Nevertheless, several conclusions may be drawn from the observed splitting patterns. We observe a first-order difference in well-constrained splitting behavior between stations located in the continental interior and those located closer to the coast. At the latter group of stations, the splitting is completely or nearly completely dominated by null measurements (Figure 5). While CBN and CNNC each have one well-constrained nonnull measurement, along with null measurements over a wide range of back azimuths, stations GOGA and NHSC exhibit only nulls. The observation of null splitting over a large swath of back azimuths is consistent with either isotropic (or nearly isotropic) mantle beneath the region, or with a vertical axis of anisotropic symmetry, as would be expected for vertical mantle flow. This argument is most clear cut for station NHSC (see Figure 5a).

[14] Farther into the continental interior, stations LRAL, TZTN, BLA, and MCWV each exhibit significant numbers of nonnull measurements, along with many nulls. For all of these stations, the fast directions cluster around an average value that is approximately NE–SW, which is roughly parallel to both the direction of absolute plate motion (APM) and the structural trend of the Appalachian Mountains. While there is some scatter in the measured splitting parameters at these stations, particularly MCWV, the splitting patterns are generally consistent with upper mantle anisotropy with a NE-SW fast axis due to shear deformation in the asthenosphere induced by the APM of North American, frozen lithospheric anisotropy associated with the Appalachian orogeny, or (most likely) a combination of the two. We note further that the nonnull measurements at LRAL, TZTN, BLA, and MCWV tend to come from northern and western back azimuths (Figures 5c and 8) and preferentially sample the mantle beneath the continental interior. Measurements from northwestern back azimuths also sample this region of the mantle, but are uniformly null at these four stations (Figure 8). These nulls are consistent with the dominantly NE-SW fast directions; SKS phases coming from the northwest will be polarized approximately 90° from the fast symmetry axis and will not be split. The roughly APM-parallel fast directions observed at these stations is consistent with the inference of *Fouch et al.* [2000] that anisotropy in this region is dominated by APM-induced mantle flow around the continental keel, with a likely additional contribution from frozen lithospheric anisotropy whose

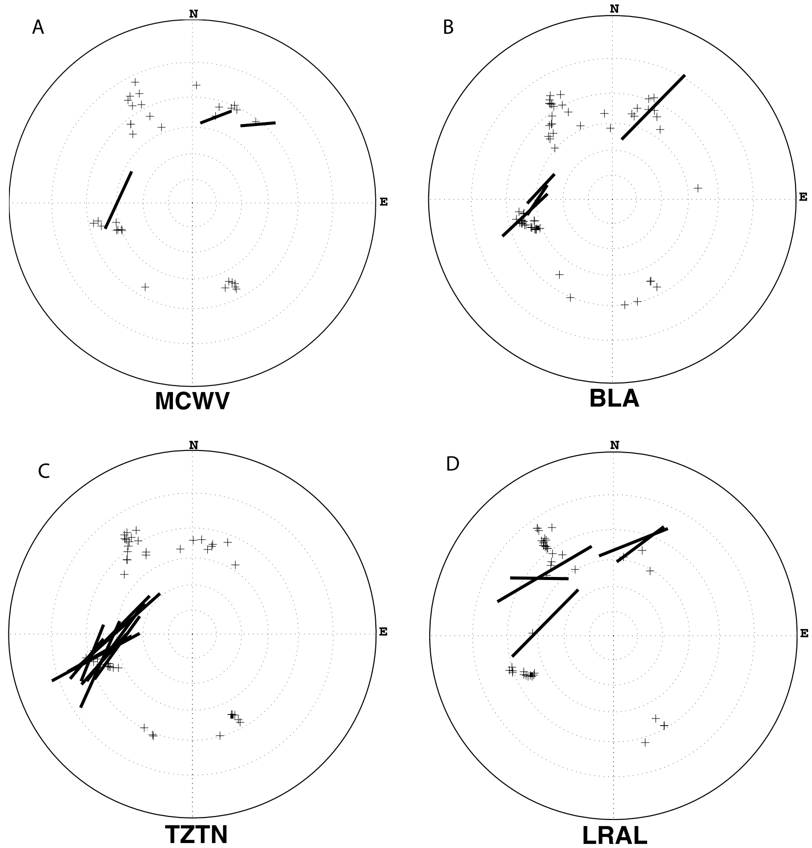

Figure 8. Splitting patterns for the four stations examined in this study that exhibited more than one nonnull measurement: (a) MCWV, (b) BLA, (c) TZTN, and (d) LRAL. Measurements are plotted on a stereographic plot with respect to the back azimuth and the incidence angle of the ray (for SKS phases, all incidence angles are close to ~10°). Nonnull measurements are plotted as bars, with the orientation and length of the bar representing the fast direction and delay time, respectively, and null measurements are plotted as crosses.

geometry is variable, but generally controlled by the orogenic history of the Appalachians.

3. Receiver Function Stacks of Mantle Discontinuity Structure: Methods and Results

[15] We examined P to S converted energy from 410 km and 660 km mantle discontinuities (hereafter referred to as the "410" and "660") beneath southeastern North America using radial receiver functions from permanent broadband stations shown in Figure 2. The 410 is usually interpreted as a mineral phase transformation from olivine to wadsleyite, and the 660 has been demonstrated to represent the phase change from ringwoodite to perovskite and magnesiowustite [e.g., *Jackson*, 1983; *Ringwood*, 1983]. Temperature variations in this region of the mantle will cause the mantle transition zone to thicken or thin because of the positive and negative Clapeyron slopes for the 410 and 660, respectively [*Bina and Helffrich*, 1994; *Ito and Katsura*, 1989]. Hydrous mantle conditions would also cause a thickening of the mantle transition zone [e.g., *Smyth and Jacobsen*, 2006]. Therefore, the relative depths of the mantle discontinuities can be used investigate the nature of mantle dynamics, but the relative contributions of temperature and hydration can be ambiguous, especially if the transition zone is thicker than average.

[16] We initially used two different methods for computing individual receiver functions to image mantle discontinuity structure: a frequency domain water level deconvolution method [e.g., *Ammon*, 1991] and a time domain deconvolution method [*Ligorría and Ammon*, 1999]. We found, however, that the water level deconvolution procedure produced receiver functions that were much less likely to have identifiable conversions from the 410 and 660 km discontinuities. Unambiguous mantle P-to-S conversions from the 410 km discontinuity using this method were only resolved at three stations:

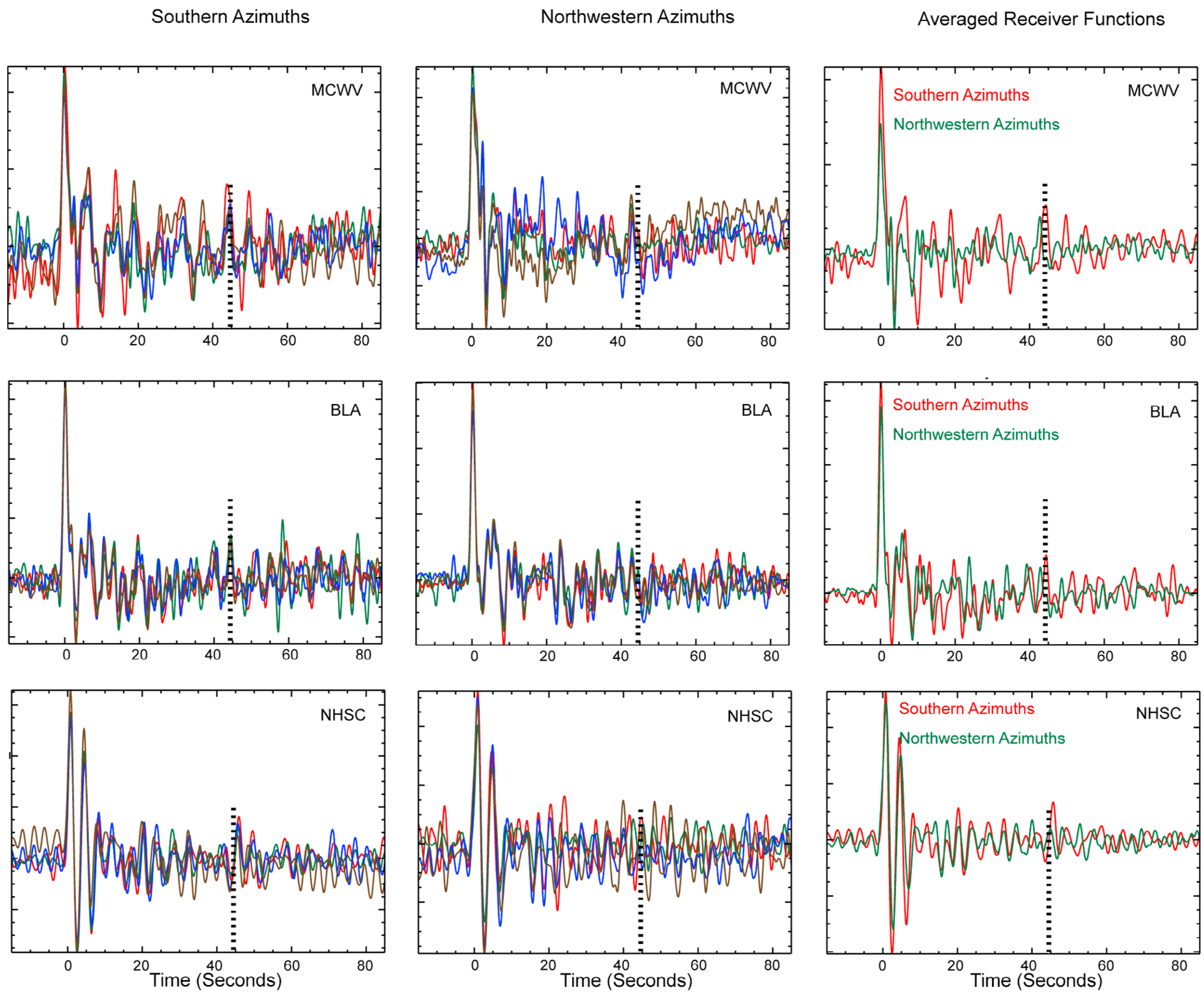

Figure 9. Receiver functions at three stations that yielded identifiable conversions from the 410 km discontinuity using the frequency domain water level deconvolution method: (top) MCWV, (middle) BLA, and (bottom) NHSC, grouped according to (left) southern back azimuths and (middle) northwestern back azimuths. (right) Comparison of the stacked receiver functions from each back azimuthal swath. The dashed line at 44 s shows the approximate expected arrival time of the signal from the mantle velocity discontinuity at 410 km depth using the PREM background model. Due to the difficulty of identifying clear arrivals from the 410 and 660 km discontinuities using this method, we mainly relied on phase-weighted stacking of receiver functions computed using time domain deconvolution in this study.

MCWV, BLA, and NHSC. These stations show coherent arrivals in the time interval 42–46 s from multiple sources (Figure 9), but the receiver functions at these stations tend to be dominated by strong, high-frequency reverberations from shallow crustal structure. This is particularly true at station NHSC, where ~750 m of unconsolidated coastal plain sediments unconformably overlie a Jurassic basalt, creating a large velocity contrast [*Chapman and Beale*, 2008]. While the signal in the time interval 42–46 s (Figure 9) is most likely due to a P-to-S conversion from the 410 km discontinuity, the difficulty in reliably identifying conversions from mantle discontinuities from the receiver functions computed with the frequency domain deconvolution method led us to rely on time domain deconvolution combined with a phase-weighted stacking algorithm to estimate transition zone thickness beneath southeastern North America.

[17] To implement this method, teleseismic P wave arrivals for earthquakes with magnitudes >6.0 were band-pass filtered between 0.15 and 5 Hz to remove microseismic and local noise, and receiver functions were computed using time domain deconvolution [*Ligorría and Ammon*, 1999] using a Gaussian parameter a = 1 (i.e., filter peak is at

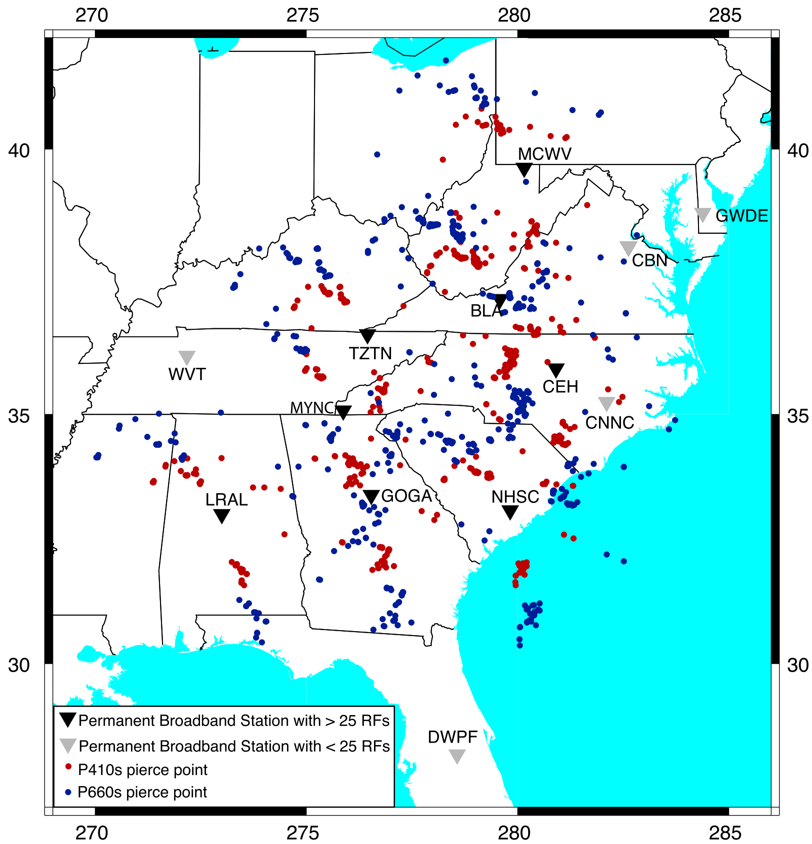

Figure 10. Map of broadband stations and pierce point locations for the 410 and 660 km discontinuities for the phase-weighted receiver function stacks shown in this study.

0.5 Hz). We experimented with different filter parameters and found that using a Gaussian parameter of a = 0.5 yielded nearly identical results. Only receiver functions that fit 80% of the signal during deconvolution were retained, and receiver functions that had large negative troughs directly preceding or following the first P arrival were discarded. The remaining receiver functions were visually inspected, and data corresponding to specific back azimuths or entire stations were discarded due excessive harmonic oscillation. Because many of the stations used in this study are either situated on thick accumulations of sedimentary rocks or unconsolidated sediments overlying crystalline basement, we anticipated that a significant amount of harmonic oscillation would be present after deconvolution due to large velocity contrasts in the crust [e.g., *Chapman and Beale*, 2008; *Cook and Vasudevan*, 2006; *McBride*, 1991], and this prediction was borne out by the data. Overall, we had to discard a large number of receiver functions due to coherent and incoherent long-period noise, though our statistical and visual selection criteria yielded similar numbers of acceptable receiver functions for each station as the statistical selection criteria used by EARS (EarthScope Automated Receiver Survey) [*Crotwell and Owens*, 2005]. Table 1 lists the number of receiver functions used in each station stack, and the 410 and 660 km pierce points for raypaths associated with receiver functions that were retained in the station stacks are shown in Figure 10.

[18] A depth correction was applied to each receiver function using the IASP91 radial velocity model [*Kennett and Engdahl*, 1991] with a local crustal correction. Variations in crustal structure were compiled from the results of several studies, including Moho depths computed by EARS [*Crotwell and Owens*, 2005], velocity variations from CRUST 2.0 [*Bassin et al.*, 2000] and several small-scale studies of regional geology [e.g., *Fnais*, 2004; *Cook and Vasudevan*, 2006]. Stacks of receiver functions were computed for each station by summing the amplitudes of the receiver functions at every 2 km in depth. We elected to produce station-averaged stacks for this study because the large distance between stations in this region of North America prohibited the use of common conversion point stacking. We did, however, examine variations in

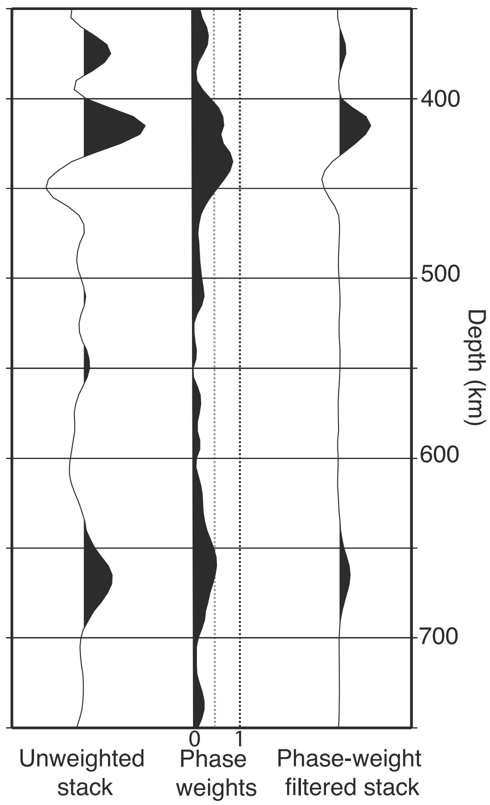

Figure 11. A demonstration of the application of the phase-weighted stacking method to the receiver function stack for station BLA. At left, the unweighted depth-migrated stack is shown. The values of the phase weights are shown in the center, and the final phase-weighted stack is shown at right. The application of the phase weighting visibly reduces long-period noise in the stacked receiver functions, particularly at depths between 400 and 700 km.

the stacks by back azimuth to examine local heterogeneity in mantle structure.

[19] We sought to remove spurious long-period noise by adopting the phase-weighting algorithm of *Schimmel and Paulssen* [1997]. This method is commonly used to remove noise from receiver function stacks of phases converted from the Moho [e.g., *Crotwell and Owens*, 2005; *Frassetto et al.*, 2010] and has been used in core-mantle boundary studies [*Helffrich and Kaneshima*, 2004], but had not been used to remove incoherent noise from stacks of mantle discontinuity structure before the present study.

[20] In this method, the amplitudes of the receiver function stack for each station are multiplied by the sums of the unit magnitudes of the instantaneous phases of the receiver functions. Using the notation of *Schimmel and Paulssen* [1997], receiver functions can be represented as

$$S(z) = s(z) + iH(s(z)) = A(z)e^{i\Phi(z)}, \quad (1)$$

where $S(z)$ represents the analytic signal of the depth (z)-converted receiver function, and $s(z)$ and $H(s(z))$ correspond to the real and Hilbert-transformed imaginary parts of the analytic signal, respectively. The sum of the components of the analytic signal can also be represented using the product of an amplitude term $A(z)$ and an instantaneous phase term $\Phi(z)$. To produce the phase weights for the stack, the values of the instantaneous phases are summed and averaged at each depth:

$$c(z) = \frac{1}{N}\left|\sum_{j=1}^{N} e^{i\Phi_j(z)}\right|, \quad (2)$$

where $c(z)$ is the mean phase weight for depth z, and N is the number of receiver functions in the stack. The final phase-weighted receiver function stack is produced by multiplying the phase weights by the amplitude of the receiver function stack at each depth z using an exponential weighting factor ν:

$$g(z) = s(z)c(z)^{\nu} \quad (3)$$

Though the weighting factor ν can be adjusted between 0 and 1 to vary the sharpness of the phase-weighted filter, we used a value of 1 to produce all of the stacks presented in this study to help eliminate the long-period noise found at most stations. Figure 11 shows an example of the phase-weighted stacking results for station BLA, where noise above 410 km and between 410 and 660 km is diminished in the phase weighted stack.

[21] Figure 10 shows the distribution of pierce points for the Pds phases at 410 and 660 km. Though events used in this study were distributed over a range of back azimuths, a large number of events were clustered to the south and northwest of the region. Figure 12 shows the station-averaged phase-weighted stacks of mantle discontinuity structure for the stations shown on the map in Figure 10. Back azimuthal variations in mantle structure were examined for each station, though only station CEH showed significant variation (>2 km) in discontinuity depth corresponding to events from southern and northwestern back azimuths. Therefore, in Figure 12 the stacked receiver functions are binned by back azimuth only for station CEH; for the rest of the stations, all back

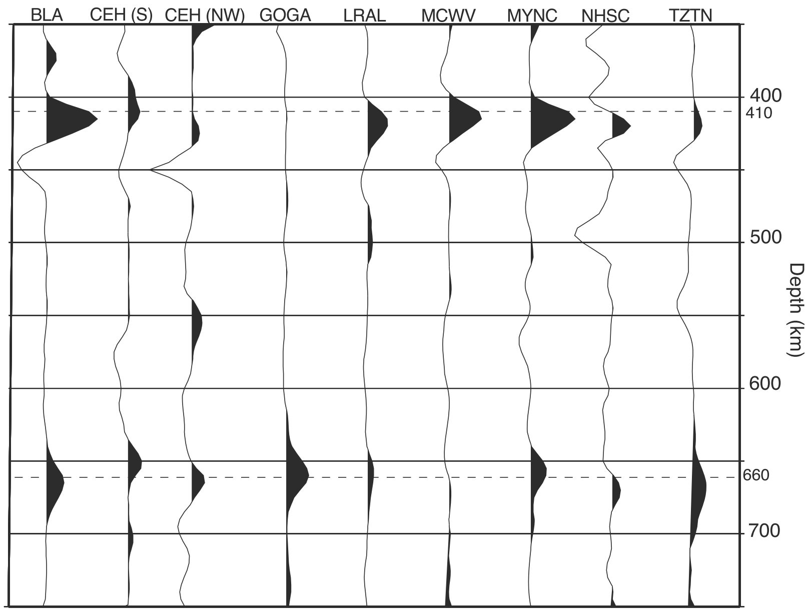

Figure 12. The final phase-weighted depth-migrated single-station stacks for eight broadband stations in the region are shown. At station CEH, a clear back azimuthal variation in the character of the receiver functions was discerned, so stacks for southerly and northwesterly back azimuths are shown separately. Clear arrivals from the 410 and 660 km discontinuities (dashed lines) can be seen at most stations.

azimuths are included in the station stack. We visually compared the phase-weighted stacks shown in Figure 12 to stacked receiver functions computed without the phase weighting, a comparison similar to that shown in Figure 11. For the non-phase-weighted stacks, we computed the 95% confidence region for each stack from the second standard deviation, which reinforces our confidence that the pulses we attribute to the 410 and 660 are statistically significant features.

[22] We note that there are significant differences between the receiver functions computed using the phase-weighted stacking algorithm with time domain deconvolution (Figure 12) and the unstacked receiver functions computed in the frequency domain shown in Figure 9. With both methods, we experimented with a variety of different filters, but more high-frequency energy was retained in Figure 9, and we also used slightly different event selection criteria for the two methods. The discrepancies between the two methods can likely be explained by a combination of these effects, as well as the more efficient suppression of low-amplitude pulses by the phase-weighted stacking method (Figure 12).

[23] Clear, unambiguous arrivals corresponding to the 410 are visible on all of the phase-weighted receiver function stacks (Figure 12) except for station GOGA, and the 410 appears to be relatively flat across the region at an average depth of 416.8 ± 4 km (Figure 13b). Station CEH in North Carolina shows a strong variation in the depth of the 410 with back azimuth; events from the south produce a stack with P-to-S conversions corresponding to 410 km depth, while events from the northwest reveal a "410" at approximately 423 km depth. Pulses corresponding to the 660 are also visible on all of the stacks except for station MCWV (Figure 12). There appears to be slightly more variability in the inferred depth of the 660 km discontinuity beneath the region, with the average depth of 661 ± 8 km (Figure 13c). Again, only station CEH showed significant variation in the depth of the 660 with back azimuth, with events from the south stacking to produce a 660 at 650 km depth and events from the northwest showing the 660 at 663 km depth. In the complete data set, the shallowest 660 at was found beneath station MYNC at 655 km depth, and the deepest was found beneath stations NHSC at 670 km depth.

[24] A plot of the transition zone thickness for each station is shown in Figure 13. Overall, the transition zone thickness is roughly uniform across the whole region, with an average thickness of 244.2 ± 5 km. This is consistent with the global average for transition zone thickness found in previous studies [e.g., *Gu et al.*, 1998; *Lawrence and Shearer*, 2006] and is also consistent with transition zone thicknesses found farther to the north for stations of the

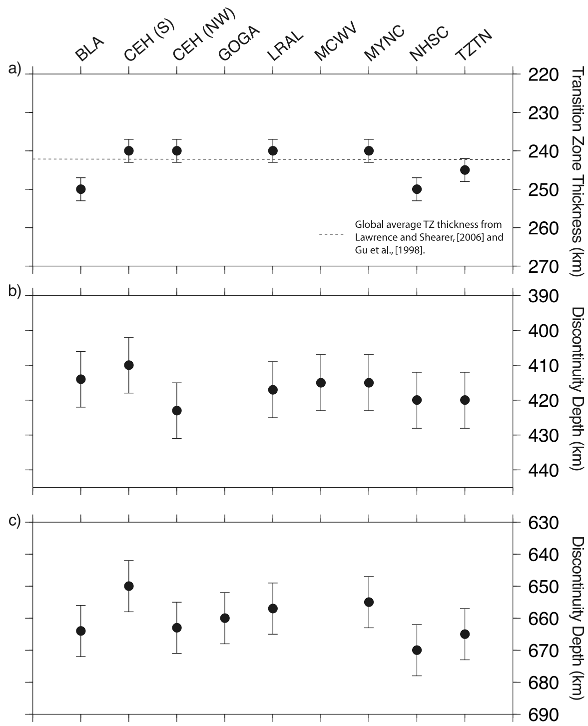

Figure 13. (a) Estimates for the average transition zone thickness derived from the estimates of the discontinuity depths for the (b) 410 and (c) 660, along with the 2σ error bars. In Figure 13a, the global average value for transition zone thickness [*Lawrence and Shearer*, 2006; *Gu et al.*, 1998] is shown as a dashed line.

Missouri-to-Massachusetts (MOMA) array [*Li et al.*, 1998]. Though station CEH shows significant variation in the relative depths of the 410 and 660, the overall transition zone thickness is the same (240 km) for stacks from both back azimuths. We do note that at two of the stations, a slight thickening of the transition zone is observed, with average thickness values for stations BLA and NHSC around 250 km. No pulse corresponding to the 520 km discontinuity is observed for the stations in the region. (This is not unexpected, as the phase-weighting algorithm used here effectively down-weights lower-amplitude signals, which should reduce the likelihood of observing smaller-amplitude reflections from P520s.) However, several of the stations do exhibit pulses between 410 and 660 km depth on the stacks shown in Figure 13; these include a large negative pulse at ~490 km at station NHSC and a positive pulse at ~550 km at station CEH (NW back azimuths). These features are not easily explained, but some caution may be warranted when interpreting the results from these stations.

[25] Error estimates for the discontinuity depths shown in Figure 13 are based on a number of factors. Estimates of the depths of discontinuities will depend heavily on the background velocity model used; our receiver function stacks were produced using the 1-D iasp91 model for mantle velocities, but any significant difference in mantle velocities beneath the southeastern United States will be a source of error in the estimates. Due to the paucity of seismic stations in the region, three-dimensional P and S velocities in the mantle are likely relatively poorly resolved, but we estimated that timing variations associated with the low Vs found throughout the upper mantle and transition zone in the NA04 model [*van der Lee and Frederiksen*, 2005] (maximum 200 m/s slower than IASP91) with Vp/Vs ratios equivalent to IASP91 would cause the errors in the depth of the 410 to be ~1.5 km and for the depth of the 660, ~3 km. If the mantle were hydrated in this region, Vp/Vs ratios are expected to be slightly elevated [e.g., *Smyth and Jacobsen*, 2006; *van der Lee and Wiens*, 2006, and references therein]. If we assume Vp/Vs ratios are 3% higher than IASP91, errors associated with NA04 model would result in average errors in the depth of the 410 of 3.5 km and 5 km for the depth of the 660 km discontinuity. Because lateral variations in Vp/Vs for the upper mantle beneath the southeastern United States are poorly resolved, however, we acknowledge that these errors may be somewhat underestimated.

[26] We also considered the possible effect of upper mantle anisotropy on the relative timing of the Ps-P phases, which might affect our estimates of the discontinuity depths. Because our shear wave splitting results suggest that the geometry of anisotropy might change significantly beneath our study area, we considered whether a change in this geometry (for example, a vertical versus horizontal fast symmetry axis) would significantly affect the relative timing of the converted phases. We used elastic constants for a typical natural peridotite rock with a maximum S anisotropy of 4% [*Mainprice*, 2007] to calculate the maximum and minimum P and S velocities that would be expected for different symmetry axis orientations. Assuming a uniform 4% anisotropy throughout the upper mantle (which is almost certainly a large overestimate, given the average shear wave splitting delay times of ~1–1.5 s observed in this study), we would expect a change in the relative arrival times of the direct P and converted S phases of no more than ~2 s for vertical versus horizontal fast symmetry axis. This corresponds to a difference in discontinuity depth of ~20 km, which is not inconsiderable; however, a more realistic model for upper mantle

anisotropy beneath the region given the relatively modest shear wave splitting delay times would invoke either a thinner anisotropic layer (~100–150 km) and/or weaker intrinsic anisotropy (~1–2%) and would be associated with smaller delay time errors (~0.5 s). Therefore, we do not expect a large effect on the estimated discontinuity depths from upper mantle anisotropy, but anisotropy may be contributing to the errors in our estimates.

[27] Insight into the effect of lateral variations in mantle velocities on estimates of the depth of transition zone discontinuities can also be gleaned by considering back azimuthal variations in the character of the receiver functions, which we observed most clearly at station CEH. Because the transition zone thickness for station CEH is the same for stacks from both the southern and northwestern back azimuths, the variations in the depths of the discontinuities are likely due to local velocity variations in the crust and upper mantle around the station. Both the 410 and 660 are inferred to lie ~13 km deeper for stacks from events to the northwest than from the south, a value that could be due to a combination of anomalously high Vp/Vs ratios for the crust and uppermost mantle (i.e., >1.85) [*Lombardi et al.*, 2009] northwest of the station or significant regional velocity anomaly that has not yet been imaged tomographically. On the whole, this result suggests that structural variations exist near this station that should be investigated further.

[28] We note, finally, that errors in the overall transition zone thickness measurements (as opposed to estimates of individual discontinuity depths) are generally insensitive to crust and upper mantle velocity variations and anisotropy and are mainly due to velocity variations within the transition zone itself. Assuming that velocity variations within the transition zone in this region are of similar magnitude as those found in model NA04 [*van der Lee and Frederiksen*, 2005], maximum errors in the thickness of the transition zone would be less than 3 km. We emphasize, however, that incomplete knowledge of lateral variations in isotropic upper mantle velocities beneath our study region may well be biasing our estimates of discontinuity depths (as opposed to transition zone thicknesses). In particular, the fact that our inferred depths of the 410 and 660 km discontinuities change across our study area and are correlated, while the calculated transition zone thicknesses are generally uniform, suggests that lateral heterogeneity in upper mantle structure in our study region is likely significant and that further velocity corrections may well be necessary once better constrained upper mantle velocity models are available.

4. Implications for Models of Mantle Flow

[29] We now consider the interpretation of our observations of shear wave splitting and transition zone discontinuity structure in the context of the models for mantle flow discussed in section 1. Because the constraints on mantle flow from shear wave splitting measurements are more direct, we consider them first. The interpretation of shear wave splitting in terms of mantle flow patterns requires knowledge of the relationship between flow and the resulting anisotropy; our knowledge of this relationship comes mainly from laboratory experiments on olivine aggregates [e.g., *Karato et al.*, 2008, and references therein]. It is usually assumed in upper mantle anisotropy studies that the fast direction tends to align with the direction of horizontal mantle flow beneath a seismic station, which is consistent with A-, C-, or E-type olivine fabric. For the case of vertical planar flow, A- or E-type fabric would result in null or small shear wave splitting, while C-type fabric would result in splitting with a fast direction normal to the shear plane [*Karato et al.*, 2008]. The presence of water in the upper mantle, which is suggested by the model of *van der Lee et al.* [2008], can result in B-type olivine fabric, which changes by 90° the relationship between flow and the fast axis of anisotropy [*Jung and Karato*, 2001]. However, B-type fabric also requires relatively low temperatures and relatively high stresses [*Karato et al.*, 2008, and references therein]. While these conditions may be found in the "cold nose" of a subduction zone mantle wedge [e.g., *Kneller et al.*, 2005, 2008], they are unlikely to be present beneath a passive continental margin. For relatively low stresses and modest temperatures, increasing water content is associated with a transition from A-type fabric to E-type to C-type, so it is possible that the upper mantle beneath our study region is dominated by E- or C-type fabric rather than the traditional A-type. Because the splitting patterns predicted for these three fabric types are generally similar, the possible presence of E- or C-type fabric due to the presence of water does not drastically change our interpretation of the results.

[30] The splitting patterns presented here do not uniquely constrain a model for mantle dynamics beneath southeastern North America, but they can

help rule out some possible models for mantle flow. The null measurements that dominate at most stations located close to the continental margin argue strongly for one of four scenarios: (1) isotropic upper mantle, (2) highly complex and vertically incoherent anisotropy [e.g., *Saltzer et al.*, 2000], (3) two layers of anisotropy producing equal time delays that are offset by ~90° and thus cancel each other out, or (4) primarily vertical flow in an A-type or E-type olivine fabric regime. We believe that the fourth scenario is most likely. It is difficult to envision a physical mechanism which could explain a region of isotropic upper mantle adjacent to the strong, APM-parallel anisotropy observed beneath the eastern U.S. continental interior in both this study and earlier work [e.g., *Fouch et al.*, 2000], since shear in the asthenosphere parallel to plate motion should result in upper mantle anisotropy everywhere beneath the plate. Forward modeling studies have demonstrated that vertically incoherent anisotropy, consisting of many anisotropic layers with varying fast directions, can produce apparent null splitting [e.g., *Saltzer et al.*, 2000]. If the lithosphere beneath the southeastern U.S. coastal plain is composed of vertically incoherent anisotropic layers, such a model could explain the null splitting we observe. It is not immediately obvious, however, why the coastal plain should have such complex anisotropy in the lithosphere compared to the mountain regions, particularly since the thicker lithosphere under the Appalachians presumably has the more complex history of assembly and deformation.

[31] We next considered the possibility of two layers of anisotropy (one in the lithosphere and one in the asthenosphere) that exhibit perfectly destructive interference. Shear wave splitting behavior in models with multiple layers of anisotropy has been extensively studied [e.g., *Silver and Savage*, 1994; *Brechner et al.*, 1998; P. G. Silver and M. D. Long, The non-commutivity of shear wave splitting operators in the low-frequency limit and implications for anisotropy tomography, submitted to *Geophysical Journal International*, 2010] and can be very complicated; the characterization of multiple layers of anisotropy can be particularly difficult for noisy data. Two layers of anisotropy with fast directions offset by exactly 90° will cancel each other out and produce no splitting, while layers offset by an angle close to but not exactly 90° should still produce significant apparent splitting for many azimuths [e.g., *Silver and Savage*, 1994]. While such a scenario cannot be completely ruled out for our data set, the presence of two anisotropic layers that nearly perfectly cancel each other out seems unlikely, particularly beneath multiple stations throughout the southeastern United States. We did consider the possibility that widespread shape-preferred orientation (SPO) of mafic dikes associated with the Triassic-Jurassic Central Atlantic Magmatic Province (CAMP) might provide a second layer of (lithospheric) anisotropy that may cancel out any APM-parallel splitting, as the stations that are dominated by null splitting tend to be located in this region. In our study area, mafic dikes associated with CAMP generally strike NNW–SSE [e.g., *McHone*, 2000] and are not, generally, perfectly orthogonal to the fast splitting directions observed farther to the west. An exception is station NHSC, beneath which CAMP-associated dikes are present and strike NW–SE. Additionally, dikes have not been mapped in the vicinity of all of the null stations observed in this study (e.g., CNNC or CBN). We consider the scenario in which SPO of CAMP dikes provides a layer of shallow anisotropy that perfectly cancels out a deeper layer of APM-parallel anisotropy to be somewhat unlikely, but the possible effect of these structures on shear wave splitting in the region deserves further study through effective medium modeling or similar techniques, and we cannot rule out this mechanism at station NHSC.

[32] The null splitting measurements observed at coastal stations are therefore, we argue, most consistent with a scenario in which mantle flow beneath the continental interior is controlled by the absolute motion of the North American plate, while mantle flow beneath the southeastern U.S. continental margin is primarily vertical. Unfortunately, the null splitting observations cannot distinguish between upgoing and downgoing mantle flow. The inference of likely vertical mantle flow beneath the southeastern U.S. continental margin is consistent with the suggestion of a mantle downwelling due to edge-driven convection [*King and Anderson*, 1998; *King*, 2007]. It is also, however, consistent with the suggestion of upward transport of water-rich mantle material beneath the eastern North American passive continental margin, as suggested by *van der Lee et al.* [2008]. We emphasize that our splitting results only argue for primarily vertical flow beneath the southeastern United States and do not shed light on the pattern of mantle flow beneath other regions of the continental margin, such as the northeastern United States. Indeed, significant splitting has been identified at New England stations that are relatively close to the coast in several previous studies [e.g., *Levin et al.*, 1999, 2000; *Fouch et al.*, 2000;

Liu, 2009]. If our inference of primarily vertical flow beneath the southeastern U.S. continental margin is correct, then there is likely a transition from vertical flow to dominantly horizontal (generally APM-parallel) flow from the southern to northern parts of the continental margin. This suggestion of along-strike changes in the geometry of mantle flow is intriguing, although its explanation is not immediately obvious.

[33] In the context of our inference of likely vertical flow beneath the continental margin from the shear wave splitting analysis, which would imply either a cold downwelling associated with edge-driven convection or a hydrated transition zone associated with the upward transport of volatiles, the observation of transition zone thicknesses that are generally consistent with the global average (Figure 13) is somewhat puzzling. Both of these models would predict thickening of the transition zone, either due to low temperatures or due to hydration, but we do not observe widespread thickening of the transition zone in this study. Of the six stations at which we were able to infer transition zone thickness, four exhibit values that are consistent with the global average (taking into account the 2σ error bars). The remaining two (BLA and NHSC) are associated with a slight thickening (~10 km) of the transition zone; this departure, while small, does appear to be significant (Figure 13). A difference in transition zone thickness of 10 km would correspond to a temperature difference of approximately 60–100 K [e.g., *Lawrence and Shearer*, 2008] if due to thermal effects. The amount of hydration that would produce a 10 km thickening of the transition zone is harder to quantify, given the limited amount of data available, but it is smaller than what would be expected for a water-saturated transition zone [e.g., *Smyth and Frost*, 2002]. The inferred ~10 km transition zone thickening can be compared to the predictions of the models considered in this paper associated with vertical flow. For the edge-driven convection scenario, a localized cold downwelling at the edge of the craton would have a temperature anomaly of perhaps ~50 K [*King and Ritsema*, 2000], which corresponds to ~5–8 km of thickening. The hydration associated with the *van der Lee et al.* [2008] model would produce ~20–40 km of transition zone thickening if the effect is due entirely to the elevation of the 410 km discontinuity under water-saturated conditions [*Smyth and Frost*, 2002]. It is notable that one of the stations associated with a thicker transition zone, NHSC, is also associated with null splitting at all back azimuths and is one of the stations for which a strong case for predominantly vertical mantle flow can be made based on the splitting observations. However, the other station which exhibits a relatively thick transition zone is BLA, which is located farther inland and is associated with several nonnull splitting measurements.

[34] The shear wave splitting measurements and receiver function analyses presented here do not allow us to identify a unique model for mantle dynamics beneath the southeastern United States. However, the data do allow us to rule out several possible models. We first note that the splitting observations are inconsistent with a scenario in which asthenospheric shear due to the motion of the North American plate dominates beneath the continental margin, as it does beneath the continental interior [*Fouch et al.*, 2000]; a transition in either the mantle flow regime or in the intrinsic anisotropy of the upper mantle is required beneath the coastal stations. We can also rule out the westward directed return flow from the Farallon slab predicted by the *Forte et al.* [2007] model, which would predict shear wave splitting with a roughly E–W fast direction at stations located throughout the southeastern United States. Of course, this does not imply that other aspects of the model are incorrect, but it does suggest that the mantle flow field beneath the southeastern North American continental margin is controlled by processes other than those modeled by *Forte et al.* [2007]. The vertical mantle flow beneath the continental margin that is strongly suggested by the splitting data is consistent with the two remaining models: that of *van der Lee et al.* [2008], which invokes the advective transport of volatiles upward through the mantle, and the edge-driven convection model [*King*, 2007], which invokes a localized downwelling at the edge of the continent. At first glance, however, neither of these models is consistent with our observation of generally average transition zone thicknesses beneath the region.

[35] How can we reconcile the inference of vertical mantle flow with the transition zone thickness observations, which appear to contradict the predictions of both the edge-driven convection model and the hydrated transition zone model? One possibility is that there is small-scale variation in the depth of transition zone discontinuities that is being obscured by the single-station stacking process. As Figure 9 demonstrates, the pierce points at the 410 and (especially) 660 km discontinuities for a given station are widely separated geographically, and single-station stacks may therefore effectively obscure any small-scale variations. Given the pos-

sibility (even likelihood) of small-scale variations in discontinuity depths if either the edge-driven convection model or the hydrated transition zone model is correct, a stacking process that takes such variability into account (such as common conversion point stacking) is desirable, but it precluded given the limited number of stations currently operating in the region. We also note that our inference of transition zone thicknesses that are close to the global average beneath the region are inconsistent with the conclusions of *Courtier and Revenaugh* [2006], who argued for a relatively shallow 410 beneath the eastern United States from multiple ScS reverberations and inferred that the transition zone is likely hydrated in this region. Again, it is possible that the sparse station coverage and single-station stacking procedure used in our study are obscuring details of transition zone structure that are visible with other types of data. Even given these uncertainties, however, we emphasize that although a model that invokes vertical flow beneath the southeastern edge of the North American continent seems to be most consistent with the splitting observations, this interpretation must be treated with some caution given the fact that our receiver function results are not consistent with the predictions of such models.

5. Outlook and Summary

[36] While it is not possible to discriminate uniquely between among different models for mantle flow using the available data, a key question is whether we will be able to uniquely constrain the pattern of mantle flow beneath southeastern North America in the future. The Transportable Array (TA) component of the ongoing USArray initiative will arrive in the southeastern United States beginning in 2012, and data from those stations and from even denser, targeted temporary experiments using the Flexible Array instrumentation will provide vastly better spatial coverage of broadband stations than is currently available. In light of these planned experiments, it is important to understand how to best exploit future data sets to understand mantle dynamics beneath the continental margin, and in our view there are several promising avenues for future progress.

[37] Unfortunately, the edge-driven convection model and the model of *van der Lee et al.* [2008] make very similar predictions for both the character of shear wave splitting and for the depth of the transition zone discontinuities: both models would predict null splitting (associated with vertical flow) and a thickened transition zone (associated with either cold temperatures or volatile enrichment). One way forward would be to examine in more detail the depth and character of both the 410 and 660 km discontinuities beneath the study region; for a water-rich transition zone, one would expect the transition zone discontinuities to broaden significantly [e.g., *van der Lee and Wiens*, 2006] and sharper discontinuities might be more consistent with a purely thermal effect. We did not observe any evidence for a broadened 410 km discontinuity in this study, which would result in the dependence of the apparent discontinuity depth and P410s amplitude on frequency, but we expect that the huge increase in the number of stations available for receiver function analysis over the next few years will allow for much tighter constraints on the character of transition zone discontinuities. The much smaller station spacing afforded by the TA will allow for common conversion point (CCP) stacking (or other stacking techniques) and will provide much better resolution of topography on the 410 and 660 km discontinuities than is possible with the sparse station coverage currently available in the southeastern United States. Additionally, we expect that the availability of TA data will allow for much better estimates of lateral variations in upper mantle velocities; because of the tradeoff between upper mantle velocity and discontinuity depth when interpreting the receiver functions, better models for upper mantle velocity heterogeneity will lead to estimates for discontinuity depths which are much more tightly constrained. Better velocity models will also help to constrain the location, extent, and strength of the low-velocity anomaly that is thought to be associated with hydrated mantle [*van der Lee et al.*, 2008]. Because of the sparse current station coverage in the southeastern United States and the lack of stations in the Atlantic Ocean to the east, the availability of data from the TA (and from denser Flexible Array-style temporary experiments) is certain to improve the resolution of velocity models and place tighter constraints on the character of this anomaly.

[38] Denser station coverage will also improve our ability to constrain the depth distribution of anisotropy beneath the eastern United States (and the relative contributions of lithospheric versus asthenospheric anisotropy) as well as the precise location of the apparent transition in splitting behavior from the continental interior to the continental margin, which in turn will place constraints on the responsible mechanism. With only 11 available long-running broadband stations in our study region, our current understanding of exactly where

the transition in shear wave splitting behavior occurs is poor. Other seismological observables that shed light on the anisotropic structure of the upper mantle beneath the region should also help to constrain the location of the transition; for example, the radial anisotropy structure, which can be gleaned from surface wave studies, would also be sensitive to a transition from horizontal to vertical mantle flow. Global and regional models of upper mantle radial anisotropy beneath the eastern United States are currently available [e.g., *Gaherty*, 2004; *Marone et al.*, 2007; *Nettles and Dziewonski*, 2008; H. Yuan et al., 3-D shear wave radially and azimuthally anisotropic velocity model of the North American upper mantle, submitted to *Geophysical Journal International*, 2010], but their lateral resolution is coarse, and it remains a challenge to properly separate the effects of radial anisotropy from the effects of crustal structure [e.g., *Ferreira et al.*, 2010]. Even given these limitations, it is interesting to note that the models of *Marone et al.* [2007] and Yuan et al. (submitted manuscript, 2010) both show radial anisotropy that is consistent with vertical flow in the general vicinity of our study region, although the radial anisotropy anomaly is not exactly colocated with our inferred region of vertical flow in the Yuan et al. (submitted manuscript, 2010) model. We expect that future surface wave investigations of both radial and azimuthal [after, e.g., *Deschamps et al.*, 2008; *Yuan and Romanowicz*, 2010; Yuan et al., submitted manuscript, 2010] anisotropy beneath the eastern United States that take advantage of dense TA data and more detailed crustal models will provide constraints complementary to those provided by shear wave splitting. Tighter constraints on the location of the possible transition from horizontal to vertical flow inferred from this study will help to constrain the responsible mechanism; for example, a transition that occurs right at the boundary of the thick continental root might be more consistent with edge-driven convection, while a transition that coincides with the boundary of the slow velocity anomaly might be more consistent with the *van der Lee et al.* [2008] model.

[39] To summarize, we have performed SKS splitting analysis and receiver function analysis at 11 permanent or long-running broadband stations in the southeastern United States in order to evaluate the predictions made by several different models for mantle dynamics beneath the continental margin. SKS splitting results reveal a pronounced transition in splitting behavior between stations located on the continental interior, which tend to exhibit mainly NE-SW fast directions with relatively large (~1.0 s) delay times, and stations located closer to the coast, which tend to be nearly or completely dominated by null measurements. The most likely explanation for this observation is a transition from mainly horizontal, APM-parallel upper mantle flow beneath the continent to mainly vertical flow (either upwelling or downwelling) beneath the passive continental margin. We identified unambiguous P-to-S conversions from the 410 and 660 km discontinuity in the receiver functions calculated for most of the stations examined. We found that calculated discontinuity depths and estimates of transition zone thicknesses derived from single-station receiver function stacks are generally consistent with global averages, with two out of six stations exhibiting evidence for slight (~10 km) thickening of the transition zone. While our seismological observations do not uniquely constrain a model for mantle flow, the splitting data strongly suggest vertical flow beneath the continental margin that may be associated with either a small-scale, edge-driven convective downwelling [*King*, 2007] or with a large-scale upwelling that transports volatiles from the deep Farallon slab to the upper mantle beneath eastern North America [*van der Lee et al.*, 2008]. However, this interpretation must be treated with some caution, as the single-station receiver function stacks calculated in this study do not show support for the widespread transition zone thickening that would be predicted by both of these models. New data from the Transportable Array and Flexible Array components of USArray should be able to distinguish between different mantle dynamics scenarios.

Acknowledgments

[40] Data used in this study are from stations of the United States National Seismic Network and were obtained from the Data Management Center (DMC) of the Incorporated Research Institutions for Seismology (IRIS). We thank Vadim Levin and Andy Frassetto for useful discussions about the eastern United States, and we are grateful to Karen Fischer, Jesse Lawrence, and the Associate Editor for thoughtful reviews that helped to improve the paper.

References

Ammon, C. J. (1991), The isolation of receiver effects from teleseismic P waveforms, *Bull. Seismol. Soc. Am.*, *81*, 2504–2510.

Barruol, G., P. G. Silver, and A. Vauchez (1997), Seismic anisotropy in the eastern United States: Deep structure of a complex continental plate, *J. Geophys. Res.*, *102*, 8329–8348, doi:10.1029/96JB03800.

Bassin, C., G. Laske, and G. Masters (2000), The current limits of resolution for surface wave tomography in North America, *Eos Trans. AGU*, *81*(48), Fall Meet. Suppl., Abstract S12A-03.

Bercovici, D., and S. Karato (2003), Whole-mantle convection and the transition-zone water filter, *Nature*, *425*, 39–44, doi:10.1038/nature01918.

Bina, C. R., and G. R. Helffrich (1994), Phase transition clapeyron slopes and transition zone seismic discontinuity topography, *J. Geophys. Res.*, *99*, 15,853–15,860, doi:10.1029/94JB00462.

Brechner, S., K. Klinge, F. Krüger, and T. Plenefisch (1998), Backazimuthal variations of splitting parameters of teleseismic SKS phases observed at the broadband stations in Germany, *Pure Appl. Geophys.*, *151*, 305–331, doi:10.1007/s000240050116.

Chapman, M. C., and J. N. Beale (2008), Mesozoic and Cenozoic faulting imaged at the epicenter of the 1886 Charleston, South Carolina earthquake, *Bull. Seismol. Soc. Am.*, *98*, 2533–2542, doi:10.1785/0120080923.

Conrad, C. P., C. Lithgow-Bertelloni, and K. E. Louden (2004), Iceland, the Farallon slab, and dynamic topography of the North Atlantic, *Geology*, *32*, 177–180, doi:10.1130/G20137.1.

Cook, F. A., and K. Vasudevan (2006), Reprocessing and enhanced interpretation of the initial COCORP Southern Appalachians traverse, *Tectonophysics*, *420*, 161–174, doi:10.1016/j.tecto.2006.01.022.

Courtier, A. M., and J. Revenaugh (2006), A water-rich transition zone beneath the eastern United States and Gulf of Mexico from multiple ScS reverberations, in *Earth's Deep Water Cycle*, *Geophys. Monogr. Ser.*, vol. 168, edited by S. D. Jacobsen and S. van der Lee, pp. 181–193, AGU, Washington, D. C.

Crotwell, H. P., and T. J. Owens (2005), Automated receiver function processing, *Seismol. Res. Lett.*, *76*, 702–709, doi:10.1785/gssrl.76.6.702.

Deschamps, F., S. Lebedev, T. Meier, and J. Trampert (2008), Stratified seismic anisotropy reveals past and present deformation beneath the east-central United States, *Earth Planet. Sci. Lett.*, *274*, 489–498, doi:10.1016/j.epsl.2008.07.058.

Farrington, R. J., D. R. Stegman, L. N. Moresi, M. Sandiford, and D. A. May (2010), Interactions of 3D mantle flow and continental lithosphere near passive margins, *Tectonophysics*, *483*, 20–28, doi:10.1016/j.tecto.2009.10.008.

Ferreira, A. M. G., J. H. Woodhouse, K. Visser, and J. Trampert (2010), On the robustness of global radially anisotropic surface wave tomography, *J. Geophys. Res.*, *115*, B04313, doi:10.1029/2009JB006716.

Fnais, M. S. (2004), The crustal and upper mantle shear velocity structure of eastern North America from the joint inversion of receiver function and surface-wave dispersion, Ph.D. thesis, Dep. of Earth and Atmos. Sci., Saint Louis Univ., St. Louis, Mo.

Forte, A. M., J. X. Mitrovica, R. Moucha, N. A. Simmons, and S. P. Grand (2007), Descent of the ancient Farallon slab drives localized mantle flow below the New Madrid seismic zone, *Geophys. Res. Lett.*, *34*, L04308, doi:10.1029/2006GL027895.

Fouch, M. J., and S. Rondenay (2006), Seismic anisotropy beneath stable continental interiors, *Phys. Earth Planet. Inter.*, *158*, 292–320, doi:10.1016/j.pepi.2006.03.024.

Fouch, M. J., K. M. Fischer, E. M. Parmentier, M. E. Wysession, and T. J. Clarke (2000), Shear wave splitting, continental keels, and patterns of mantle flow, *J. Geophys. Res.*, *105*, 6255–6275, doi:10.1029/1999JB900372.

Frassetto, A., G. Zandt, H. Gilbert, T. J. Owens, and C. Jones (2010), Improved imaging with phase-weighted common conversion point stacks of receiver functions, *Geophys. J. Int.*, *182*, 368–374.

Gaherty, J. B. (2004), A surface wave analysis of seismic anisotropy beneath eastern North America, *Geophys. J. Int.*, *158*, 1053–1066, doi:10.1111/j.1365-246X.2004.02371.x.

Grana, J. P., and R. M. Richardson (1996), Tectonic stresses within the New Madrid seismic zone, *J. Geophys. Res.*, *101*, 5445–5458, doi:10.1029/95JB03255.

Gu, Y. J., A. M. Dziewonski, and C. B. Agee (1998), Global de-correlation of the topography of transition zone discontinuities, *Earth Planet. Sci. Lett.*, *157*, 57–67, doi:10.1016/S0012-821X(98)00027-2.

Helffrich, G., and S. Kaneshima (2004), Seismological constraints on core composition from Fe-O-S liquid immiscibility, *Science*, *306*, 2239–2242, doi:10.1126/science.1101109.

Higo, Y., T. Inoue, T. Irifune, and H. Yurimoto (2001), Effect of water on the spinel-postspinel transformation in Mg_2SiO_4, *Geophys. Res. Lett.*, *28*, 3505–3508, doi:10.1029/2001GL013194.

Ito, E., and T. Katsura (1989), A temperature profile of the mantle transition zone, *Geophys. Res. Lett.*, *16*, 425–428, doi:10.1029/GL016i005p00425.

Jackson, I. (1983), Some geophysical constraints on the chemical composition of the Earth's lower mantle, *Earth Planet. Sci. Lett.*, *62*, 91–103, doi:10.1016/0012-821X(83)90073-0.

Jung, H., and S. Karato (2001), Water-induced fabric transitions in olivine, *Science*, *293*, 1460–1463, doi:10.1126/science.1062235.

Karato, S., H. Jung, I. Katayama, and P. Skemer (2008), Geodynamic significance of seismic anisotropy of the upper mantle: New insights from laboratory studies, *Annu. Rev. Earth Planet. Sci.*, *36*, 59–95, doi:10.1146/annurev.earth.36.031207.124120.

Kennett, B. L. N., and E. R. Engdahl (1991), Traveltimes for global earthquake location and phase identification, *Geophys. J. Int.*, *105*, 429–465, doi:10.1111/j.1365-246X.1991.tb06724.x.

King, S. D. (2007), Hotspots and edge-driven convection, *Geology*, *35*, 223–226, doi:10.1130/G23291A.1.

King, S. D., and D. L. Anderson (1998), Edge-driven convection, *Earth Planet. Sci. Lett.*, *160*, 289–296, doi:10.1016/S0012-821X(98)00089-2.

King, S. D., and J. Ritsema (2000), African hotspot volcanism: Small-scale convection in the upper mantle beneath cratons, *Science*, *290*, 1137–1140, doi:10.1126/science.290.5494.1137.

Kneller, E. A., P. E. van Keken, S. Karato, and J. Park (2005), B-type olivine fabric in the mantle wedge: Insights from high-resolution non-Newtonian subduction zone models, *Earth Planet. Sci. Lett.*, *237*, 781–797, doi:10.1016/j.epsl.2005.06.049.

Kneller, E. A., M. D. Long, and P. E. van Keken (2008), Olivine fabric transitions and shear wave anisotropy in the Ryukyu subduction system, *Earth Planet. Sci. Lett.*, *268*, 268–282, doi:10.1016/j.epsl.2008.01.004.

Lawrence, J. F., and P. M. Shearer (2006), A global study of transition zone thickness using receiver functions, *J. Geophys. Res.*, *111*, B06307, doi:10.1029/2005JB003973.

Lawrence, J. F., and P. M. Shearer (2008), Imaging mantle transition zone thickness with SdS-SS finite-frequency sensitivity kernels, *Geophys. J. Int.*, *174*, 143–158, doi:10.1111/j.1365-246X.2007.03673.x.

Levin, V., W. Menke, and J. Park (1999), Shear wave splitting in the Appalachians and the Urals: A case for multilayered anisotropy, *J. Geophys. Res.*, *104*, 17,975–17,993, doi:10.1029/1999JB900168.

Levin, V., J. Park, M. T. Brandon, and W. Menke (2000), Thinning of the upper mantle during late Paleozoic Appalachian orogenesis, *Geology*, *28*, 239–242, doi:10.1130/0091-7613(2000)28<239:TOTUMD>2.0.CO;2.

Li, A., K. M. Fischer, M. E. Wysession, and T. J. Clarke (1998), Mantle discontinuities and temperature under the North American continental keel, *Nature*, *395*, 160–163, doi:10.1038/25972.

Ligorría, J. P., and C. J. Ammon (1999), Iterative deconvolution and receiver function estimation, *Bull. Seismol. Soc. Am.*, *89*, 1395–1400.

Liu, K. H. (2009), NA-SWS-1.1: A uniform database of teleseismic shear wave splitting measurements for North America, *Geochem. Geophys. Geosyst.*, *10*, Q05011, doi:10.1029/2009GC002440.

Liu, L., S. Spasojevic, and M. Gurnis (2008), Reconstructing Farallon plate subduction beneath North America back to the late Cretaceous, *Science*, *322*, 934–938, doi:10.1126/science.1162921.

Lombardi, D., J. Braunmiller, E. Kissling, and D. Giardini (2009), Alpine mantle transition zone imaged by receiver functions, *Earth Planet. Sci. Lett.*, *278*, 163–174, doi:10.1016/j.epsl.2008.11.029.

Long, M. D., and P. G. Silver (2009), Shear wave splitting and mantle anisotropy: Measurements, interpretations, and new directions, *Surv. Geophys.*, *30*, 407–461, doi:10.1007/s10712-009-9075-1.

Long, M. D., and R. D. van der Hilst (2005), Estimating shear wave splitting parameters from broadband recordings in Japan: A comparison of three methods, *Bull. Seismol. Soc. Am.*, *95*, 1346–1358, doi:10.1785/0120040107.

Long, M. D., H. Gao, A. Klaus, L. S. Wagner, M. J. Fouch, D. E. James, and E. D. Humphreys (2009), Shear wave splitting and the pattern of mantle flow beneath eastern Oregon, *Earth Planet. Sci. Lett.*, *288*, 359–369, doi:10.1016/j.epsl.2009.09.039.

Mainprice, D. (2007), Seismic anisotropy of the deep Earth from a mineral and rock physics perspective, in *Treatise on Geophysics*, vol. 2, *Mineral Physics*, edited by G. Schubert, pp. 437–491, doi:10.1016/B978-044452748-6.00045-6, Elsevier, Amsterdam.

Marone, F., Y. Gung, and B. Romanowicz (2007), Three-dimensional radial anisotropic structure of the North American upper mantle from inversion of surface wave data, *Geophys. J. Int.*, *171*, 206–222, doi:10.1111/j.1365-246X.2007.03465.x.

McBride, J. H. (1991), Constraints on the structure and tectonic development of the early Mesozoic South Georgia Rift, southeastern United States: Seismic reflection data processing and interpretation, *Tectonics*, *10*, 1065–1083, doi:10.1029/90TC02682.

McHone, J. G. (2000), Non-plume magmatism and tectonics during the opening of the central Atlantic Ocean, *Tectonophysics*, *316*, 287–296, doi:10.1016/S0040-1951(99)00260-7.

Moucha, R., A. M. Forte, J. X. Mitrovica, D. B. Rowley, S. Quéré, N. A. Simmons, and S. P. Grand (2008), Dynamic topography and long-term sea-level variations: There is no such thing as a stable continental platform, *Earth Planet. Sci. Lett.*, *271*, 101–108, doi:10.1016/j.epsl.2008.03.056.

Nettles, M., and A. M. Dziewonski (2008), Radially anisotropic shear velocity structure of the upper mantle globally and beneath North America, *J. Geophys. Res.*, *113*, B02303, doi:10.1029/2006JB004819.

Pozgay, S., D. A. Wiens, J. A. Conder, H. Shiobara, and H. Sugioka (2007), Complex mantle flow in the Mariana subduction system: Evidence from shear wave splitting, *Geophys. J. Int.*, *170*, 371–386, doi:10.1111/j.1365-246X.2007.03433.x.

Ringwood, A. E. (1983), *Composition and Petrology of the Earth's Mantle*, McGraw-Hill, New York.

Saltzer, R. L., J. Gaherty, and T. H. Jordan (2000), How are vertical shear wave spitting measurements affected by variations in the orientation of azimuthal anisotropy with depth?, *Geophys. J. Int.*, *141*, 374–390, doi:10.1046/j.1365-246x.2000.00088.x.

Schimmel, M., and H. Paulssen (1997), Noise reduction and detection of weak, coherent signals through phase-weighted stacks, *Geophys. J. Int.*, *130*, 497–505, doi:10.1111/j.1365-246X.1997.tb05664.x.

Silver, P. G., and M. K. Savage (1994), The interpretation of shear wave splitting parameters in the presence of two anisotropic layers, *Geophys. J. Int.*, *119*, 949–963, doi:10.1111/j.1365-246X.1994.tb04027.x.

Smyth, J. R., and D. J. Frost (2002), The effect of water on the 410-km discontinuity: An experimental study, *Geophys. Res. Lett.*, *29*(10), 1485, doi:10.1029/2001GL014418.

Smyth, J. R., and S. D. Jacobsen (2006), Nominally anhydrous minerals and Earth's deep water cycle, in *Earth's Deep Water Cycle*, *Geophys. Monogr. Ser.*, vol. 168, edited by S. D. Jacobsen and S. van der Lee, pp. 1–11, AGU, Washington, D. C.

Spasojevic, S., M. Gurnis, and R. Sutherland (2010), Mantle upwellings above slab graveyards linked to the global geoid lows, *Nat. Geosci.*, *3*, 435–438, doi:10.1038/ngeo855.

van der Lee, S., and A. Frederiksen (2005), Surface wave tomography applied to the North America upper mantle, in *Seismic Earth: Array Analysis of Broadband Seismograms*, *Geophys. Monogr. Ser.*, vol. 157, edited by G. Nolet and A. Levander, pp. 67–80, AGU, Washington, D. C.

van der Lee, S. K., and D. A. Wiens (2006), Seismological constraints on Earth's deep water cycle, in *Earth's Deep Water Cycle*, *Geophys. Monogr. Ser.*, vol. 168, edited by S. D. Jacobsen and S. van der Lee, pp. 13–27, AGU, Washington, D. C.

van der Lee, S., K. Regenauer-Lieb, and D. A. Yuen (2008), The role of water in connecting past and future episodes of subduction, *Earth Planet. Sci. Lett.*, *273*, 15–27, doi:10.1016/j.epsl.2008.04.041.

Wood, B. (1995), The effect of H_2O on the 410-kilometer seismic discontinuity, *Science*, *268*, 74–76, doi:10.1126/science.268.5207.74.

Wüstefeld, A., and G. Bokelmann (2007), Null detection in shear-wave splitting measurements, *Bull. Seismol. Soc. Am.*, *97*, 1204–1211, doi:10.1785/0120060190.

Wüstefeld, A., G. Bokelmann, G. Barruol, and C. Zaroli (2008), Splitlab: A shear-wave splitting environment in Matlab, *Comput. Geosci.*, *34*, 515–528, doi:10.1016/j.cageo.2007.08.002.

Yuan, H., and B. Romanowicz (2010), Lithospheric layering in the North American craton, *Nature*, *466*, 1063–1068, doi:10.1038/nature09332.